ChemComm

COMMUNICATION

View Article Online
View Journal | View Issue



Cite this: *Chem. Commun.*, 2024, **60**, 14774

Received 9th October 2024,
Accepted 15th November 2024

DOI: 10.1039/d4cc05331a

rsc.li/chemcomm



# A cobalt-tetraphenylporphyrin-based hypercrosslinked polymer for efficient $CO_2$ photoreduction to CO†

Saif Ullah,[a] Xunliang Hu,[a] Yaqin Zhang,[a] Irshad Hussain,[b] Xiaoyan Wang,[a] Hui Gao*[a] and Bien Tan*[a]

**One of the main impediments during the $CO_2$ photocatalytic reduction process is controlling a particular product's selectivity while keeping a high conversion rate. The adsorption and affinity of the catalyst for $CO_2$ are key factors for achieving highly efficient $CO_2$ reduction. Herein, we report a novel photocatalytic material, cobalt anchored onto a tetraphenylporphyrin-based hypercrosslinked polymer (HCP-CoTPP), which was designed for the efficient photoreduction of $CO_2$ to CO with an impressive evolution rate of 1449.9 μmol $g^{-1}$ $h^{-1}$ and nearly 100% selectivity in the presence of $[Ru(Bpy)_3]Cl_2$ as a photosensitizer and sacrificial agent under visible light irradiation.**

Photocatalytic $CO_2$ reduction is a compelling method for simultaneously utilizing solar energy and converting $CO_2$ into valuable products.[1,2] Substantial efforts have been dedicated to developing photocatalytic systems that can convert $CO_2$ into a specific product efficiently.[3] For efficient $CO_2$ conversion, a system should ideally provide a platform with abundant catalytic centers and high porosity to support charge and mass transfer. This can be efficiently achieved by integrating catalytic sites into porous materials: the porosity promotes $CO_2$ adsorption, while the catalytic sites facilitate its conversion.[4,5]

In recent years, various porous materials such as metal–organic frameworks (MOFs), covalent organic frameworks (COFs), and conjugated microporous polymers (CMPs) have demonstrated significant promise in constructing efficient photocatalytic $CO_2$ reduction systems.[6–8] Recently, Zheng *et al.*[9] reported that photocatalytic $CO_2$ reduction using GO-COF-366-Co achieved a CO selectivity of 96.1% and a yield of 52.2 mmol $g^{-1}$. Rahimi *et al.*[10] reported that compared to the non-donor 1,3,5-triethynylbenzene-based TEB-GFP CMP, photocatalytic $CO_2$ reduction using a donor–acceptor based TPA-GFP CMP resulted in a 3-fold increase in CO evolution yield, reaching a maximum CO yield of 1666 μmol $g^{-1}$ $h^{-1}$ at 12 hours, and the selectivity improved significantly from 54% in TEB-GFP to 95% in TPA-GFP. However, these materials suffer from limitations such as high cost and difficult scalability.[9,11–17] Hypercrosslinked polymers (HCPs), a class of porous organic polymers, are characterized by high surface area, tunable porosity, cost-effectiveness, ease of functionalization, and exceptional stability.[18–21] Additionally, HCPs are ideal for incorporating catalytic sites, enabling the development of multiphase catalytic systems, making them highly promising for $CO_2$ conversion applications.[22–24] The effectiveness of $CO_2$ conversion is closely linked to a material's $CO_2$ capture ability.[25] Materials with low adsorption capacities often suffer from reduced $CO_2$ concentrations at the catalytic sites.[26] However, most metal-based HCPs reported to date exhibit insufficient $CO_2$ adsorption, leading to poor utilization of $CO_2$.[20,27,28] In this study, a tetraphenylporphyrin-based HCP (HCP-TPP) was synthesized *via* a Friedel–Crafts alkylation reaction. The heteroatoms in the porphyrin moiety exhibit $CO_2$-philic properties, enhancing $CO_2$ adsorption.[29–32] Meanwhile, the porphyrin unit, recognized as a metal coordination site, facilitates the incorporation of metal ions, which act as catalytic centers while preventing metal ion agglomeration. Cobalt ions were subsequently introduced into the pores of HCP-TPP, enabling the photoreduction of $CO_2$ to CO.[33–35] The photocatalytic system exhibited outstanding photocatalytic performance, achieving a CO evolution rate of 1449.9 μmol $g^{-1}$ $h^{-1}$ with nearly 100% selectivity under visible light in the presence of Ru dye.[12,36]

The tetraphenylporphyrin-based HCP (HCP-TPP) was prepared *via* Friedel–Crafts alkylation reaction by the solvent kitting strategy under a nitrogen atmosphere with the

[a] *Key Laboratory of Material Chemistry for Energy Conversion and Storage Ministry of Education, Hubei Key Laboratory of Material Chemistry and Service Failure, School of Chemistry and Chemical Engineering, Huazhong University of Science and Technology, Luoyu Road No. 1037, Wuhan, 430074, P. R. China. E-mail: bien.tan@mail.hust.edu.cn*

[b] *Department of Chemistry & Chemical Engineering, SBA School of Science & Engineering, Lahore University of Management Sciences (LUMS), DHA, Lahore Cantt, Lahore 54792, Pakistan*

† Electronic supplementary information (ESI) available: Experimental details, and additional characterization figures. See DOI: https://doi.org/10.1039/d4cc05331a

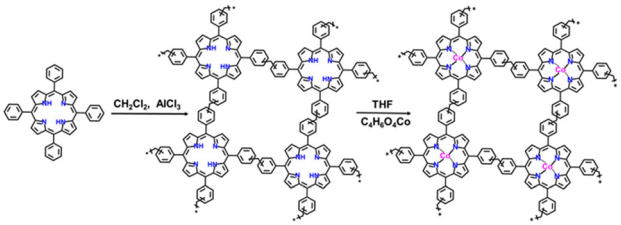


Fig. 1 Synthesis of a cobalt-tetraphenylporphyrin-based hyper cross-linked polymer.

temperature gradually increased from 0 °C to 80 °C (see ESI† for experimental details). Cobalt ions were introduced into the HCP-TPP by a simple treatment of HCP-TPP with cobalt acetate, yielding HCP-CoTPP (Fig. 1).[28] The chemical structures of HCP-TPP and HCP-CoTPP were analyzed by Fourier transform infrared (FT-IR) spectroscopy (Fig. 2a), and the bands at 1600 $cm^{-1}$, 1500 $cm^{-1}$, and 1450 $cm^{-1}$ are assigned to the aromatic ring structure. The peaks in the area of 2920–2960 $cm^{-1}$ are attributed to the characteristic aliphatic C–H stretching vibrations of the methylene group, implying the success of the Friedel–Crafts alkylation.[37]

Solid-state $^{13}C$ cross polarization/magic angle spinning (CP/MAS) NMR spectroscopy was used to further confirm the chemical structure of HCP-CoTPP. The carbon atoms of the methylene groups are responsible for resonance peaks at about 52 ppm. Furthermore, the resonance peak assigned at 130 ppm due to the presence of aromatic carbon confirms the tetraphenylporphyrin structure (Fig. 2b).[38]

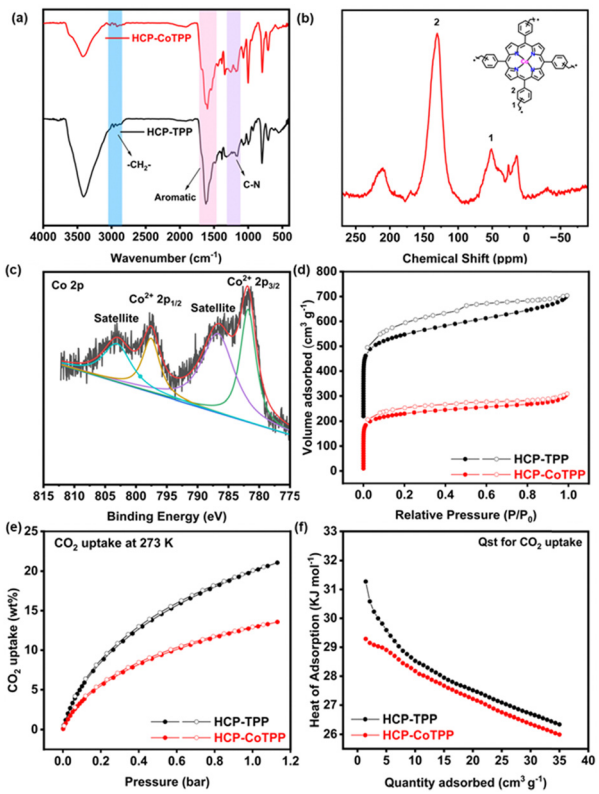


Fig. 2 (a) FT-IR spectra of HCP-TPP and HCP-CoTPP, (b) solid-state $^{13}C$ NMR spectra of HCP-CoTPP, (c) XPS spectra for Co 2p of HCP-CoTPP, (d) nitrogen adsorption–desorption isotherms of HCPs at 77.3 K, (e) $CO_2$ adsorption–desorption isotherm of HCPs at 273 K 1.13 bar, and (f) isosteric heat of adsorption of HCP-TPP and HCP-CoTPP.

The chemical state of the Co was determined by X-ray photoelectron spectroscopy (XPS) (Fig. 2c). The binding energy peaks at 797.5 and 781.9 eV are assigned to $Co^{2+}$ $2p_{1/2}$ and $Co^{2+}$ $2p_{3/2}$, respectively, confirming that the valence state of the cobalt ion is +2 and the cobalt ions are successfully loaded into the tetraphenylporphyrin.[39,40] The thermogravimetric analysis (TGA) of HCP-TPP and HCP-CoTPP under nitrogen demonstrated their good thermal stability (Fig. S1, ESI†). The initial mass loss observed below 100 °C is primarily due to the presence of the entrapped gases and moisture in the high surface area HCPs. Scanning electron microscope (SEM) images show that the HCP-CoTPP has an irregular bulk morphology (Fig. S2, ESI†). The energy-dispersive X-ray spectroscopy (EDX) elemental mapping demonstrated the homogeneous distribution of cobalt ions in HCP-CoTPP. The cobalt content, as measured by ICP-OES analysis, is 3.5 wt%.

The porous properties of the HCPs were analysed by nitrogen sorption analysis at 77.3 K. The detailed Brunauer–Emmett–Teller (BET) surface area, pore volumes, and micropore volumes of the materials are summarised in Table S1 (ESI†). The specific surface areas of the HCP-TPP and HCP-CoTPP were 1239 and 861 $m^2\ g^{-1}$, respectively. As illustrated in Fig. 2d, the adsorption isotherms of all samples exhibit a sharp nitrogen gas uptake at low relative pressure ($P/P_0 < 0.01$), implying the presence of microporosity. The hysteresis loop at the medium pressure region ($P/P_0$ = 0.4–0.7) reveals mesopores in the samples. The pore size distribution, calculated by nonlocal density functional theory (NLDFT), also confirms thepresence of micropores and mesopores in HCP-TPP and HCP-CoTPP (Fig. S3, ESI†). $CO_2$ uptake capability is an important parameter for highly efficient $CO_2$ conversion. As shown in Fig. 2e, HCP-TPP exhibits the $CO_2$ adsorption capability of 21.9 wt% (1.13 bar, 273 K) and 13.5 wt% (1.13 bar, 298 K). The incorporation of $Co^{2+}$ ions into HCP-TPP led to a reduction in $CO_2$ adsorption capacity, primarily due to a decrease in specific surface area and micropore volume. The $CO_2$ uptake of HCP-CoTPP decreased to 13.1 wt% at 1.13 bar/273 K and 8.2 wt% at 1.13 bar/298 K (Fig. S4 and Table S2, ESI†). To gain deeper insight into the adsorption interactions between tetraphenylporphyrin-based HCPs and $CO_2$ molecules, the isosteric heat of adsorption ($Q_{st}$) was calculated from $CO_2$ adsorption isotherms at 273 K and 298 K using the Clausius–Clapeyron equation (Fig. 2f). The onset $Q_{st}$ values of HCP-TPP and HCP-CoTPP were 31.2 and 29.2 kJ $mol^{-1}$, respectively, which is higher than that of the most of the porous organic polymers, such as TpBpy-COF (22 kJ $mol^{-1}$), Por-$sp^2$c-COF (25 kJ $mol^{-1}$) and PCP-Cl (27 kJ $mol^{-1}$).[41–43] The high $Q_{st}$ values indicate strong interactions and high affinity between $CO_2$ and the tetraphenylporphyrin-based HCPs, which promotes subsequent conversion reactions.

Given the catalytic properties of Co–ligand complexes for $CO_2$ reduction and the high $CO_2$ affinity of HCP-CoTPP, we evaluated the photocatalytic $CO_2$ conversion activity of HCP-CoTPP.

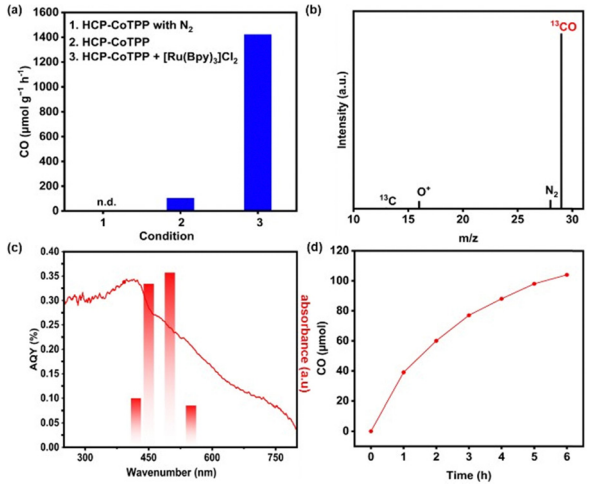


Fig. 3 (a) The photocatalytic $CO_2$ conversion rate under different conditions using CoTPP as a catalyst and visible light irradiation ($\lambda \geq 420$ nm). Condition 1: under $N_2$, conditions 2 and 3: under $CO_2$, (b) mass spectrum of $^{13}CO$ produced using HCP-CoTPP as the catalyst in the photocatalytic reduction of $^{13}CO_2$, (c) apparent quantum yield (AQY) of $CO_2$ photocatalytic reduction for HCP-CoTPP at different wavelengths, (d) CO evolution by HCP-CoTPP (10 mg) with the presence of $[Ru(Bpy)_3]Cl_2$ = (10 mg) within 6 hours.

This was performed in the presence of $[Ru(Bpy)_3]Cl_2$ (Bpy = 2,2′-bipyridine) as a visible-light photosensitizer and triethanolamine (TEOA) as a hole-sacrificial reagent, in an acetonitrile/aqueous solution under visible light irradiation ($\lambda \geq 420$ nm, 300 W Xe light source). HCP-CoTPP exhibited the CO evolution rate of 103.6 μmol $g^{-1}$ $h^{-1}$, while with $[Ru(Bpy)_3]Cl_2$, the CO evolution rate was 1449.9 μmol $g^{-1}$ $h^{-1}$ (Fig. 3a). When DMF was used as the solvent, the photocatalytic efficiency was improved to 2579.9 μmol $g^{-1}$ $h^{-1}$ (Fig. S5, ESI†). The $H_2$ evolution is negligible, which gives nearly 100% selectivity. The photocatalytic performance of HCP-CoTPP is comparable with other previously reported porous organic photocatalysts (Table S3, ESI†).

Control experiments were carried out by replacing the $CO_2$ with $N_2$, in which CO was not detected in the photocatalytic reaction under similar conditions either with or without photosensitizer (Fig. 3a). To confirm the origin of CO, an isotope labeling study was conducted using $^{13}CO_2$ as a carbon source. The peak at $m/z$ = 29 indicates that the generated $^{13}CO$ is from $^{13}CO_2$, demonstrating that the $^{13}CO$ evolution from $^{13}CO_2$ not from the decomposition of any other organic compounds in the photocatalytic system (Fig. 3b). Apparent quantum yield (AQY) was measured at different wavelengths, showing 0.10% at 420 nm, 0.33% at 450 nm, 0.35% at 500 nm, and 0.08% at 550 nm (Fig. 3c). Furthermore, CO production continued for up to 6 hours, indicating that the catalyst remains stable during the photocatalytic reaction system (Fig. 3d). HCP-CoTPP demonstrates excellent durability, achieving a high yield of CO evolution over 24 hours under visible light irradiation (Fig. S6, ESI†). From the NMR spectra of the reaction solution (Fig. S7 and S8, ESI†), no carbon-containing products were detected in the reaction solution.

A possible reaction mechanism for the photocatalytic reduction of $CO_2$ over HCP-CoTPP is proposed (Fig. S9, ESI†). The process involves the photoexcitation of $[Ru(Bpy)_3]Cl_2$ under light irradiation, generating excited electrons and holes. The excited electrons are transferred to the HCP-CoTPP and coupled with $CO_2$ to produce CO. The holes are reductively quenched by TEOA.[39,44,45]

In conclusion, the cobalt-tetraphenylporphyrin-based HCP was prepared by a simple two-step strategy. HCP-CoTPP exhibited high $CO_2$ uptake (13.1 wt% at 273 K, 1.13 bar), strong interaction ($Q_{st}$: 29.2 kJ $mol^{-1}$) and high affinity with $CO_2$, and had abundant catalytic sites. The photocatalytic $CO_2$ reduction by HCP-CoTPP is efficient in the presence of photosensitizer and a hole-sacrificial reagent. This photocatalytic system demonstrated a CO evolution rate of 1449.9 μmol $g^{-1}$ $h^{-1}$, and selectivity nearly 100% under visible light. This study demonstrates that the good $CO_2$ uptake and high affinity to $CO_2$ improve its photocatalytic conversion efficiency, providing new insight for developing highly efficient $CO_2$ photocatalytic systems.

The authors acknowledge the assistance of the Analysis and Testing Center team at Huazhong University of Science and Technology for their support in material characterization. This work was financially supported by the National Natural Science Foundation of China (Grant No. 22161142005, 22475076) and National Key R&D Program of China (2023YFB4104000).

## Data availability

The data supporting this article have been included as part of the ESI.†

## Conflicts of interest

There are no conflicts to declare.

## Notes and references

1 A. Rawat, A. Kumar, A. Pal, D. Arukha, P. Joshi and P. Mohanty, *ACS Appl. Nano Mater.*, 2024, 7, 3761–3773.
2 P. Joshi, S. Mehta, N. Singh, S. Dalakoti, S. Divekar, S. Dasgupta, M. Srivastava and O. P. Khatri, *J. Environ. Chem. Eng.*, 2023, **11**, 110291.
3 S. Wang, X. Hai, X. Ding, S. Jin, Y. Xiang, P. Wang, B. Jiang, F. Ichihara, M. Oshikiri and X. Meng, *Nat. Commun.*, 2020, **11**, 1149.
4 A. Rawat, R. Muhammad, V. Chandra Srivastava and P. Mohanty, *Macromolecules*, 2023, **56**, 1236–1242.
5 J. Li, K. Ma, Y. He, S. Ren, C. Li, X.-B. Chen, Z. Shi and S. Feng, *Catal. Sci. Technol.*, 2021, **11**, 7300–7306.
6 M. Zhang, P. Huang, J. P. Liao, M. Y. Yang, S. B. Zhang, Y. F. Liu, M. Lu, S. L. Li, Y. P. Cai and Y. Q. Lan, *Angew. Chem., Int. Ed.*, 2023, **62**, e202311999.
7 K. Seob Song, P. W. Fritz, D. F. Abbott, L. Nga Poon, C. M. Caridade, F. Gándara, V. Mougel and A. Coskun, *Angew. Chem., Int. Ed.*, 2023, **62**, e202309775.
8 Z. Ding, X. Tang, D. Zhao, S. Yan, L. Li, P. Li, W. Tang, S.-Y. Zhang and Y.-J. Zeng, *Inorg. Chem.*, 2024, **63**, 14193–14199.
9 Y. N. Gong, J. H. Mei, W. J. Shi, J. W. Liu, D. C. Zhong and T. B. Lu, *Angew. Chem., Int. Ed.*, 2024, **63**, e202318735.
10 F. A. Rahimi, A. Singh, R. Jena, A. Dey and T. K. Maji, *ACS Appl. Mater. Interfaces*, 2024, **16**, 43171–43179.
11 J. Yang, Z. Chen, L. Zhang and Q. Zhang, *ACS Nano*, 2024, **18**, 21804–21835.

 

12 D. H. Streater, E. R. Kennehan, D. Wang, C. Fiankor, L. Chen, C. Yang, B. Li, D. Liu, F. Ibrahim and I. Hermans, *J. Am. Chem. Soc.*, 2024, **146**, 4489–4499.
13 K. Sun, Y. Huang, Q. Wang, W. Zhao, X. Zheng, J. Jiang and H.-L. Jiang, *J. Am. Chem. Soc.*, 2024, **146**, 3241–3249.
14 Y. Zheng, X. Shen, M. Lin, M. Zhu, B. Yang, J. Yan, Z. Zhuang and Y. Yu, *Small*, 2024, **20**, 2306836.
15 N. Li, G.-Q. Lai, L.-H. Chung, F. Yu, J. He and Y.-Q. Lan, *CCS Chem.*, 2024, **6**, 1211–1221.
16 P. Chakrabortty, S. Ghosh, R. V. Singh, M. R. Pai, K. Yusuf and S. M. Islam, *ACS Sustainable Chem. Eng.*, 2024, **12**, 10978–10992.
17 R. K. Saravanan, S. Karmakar, F. A. Rahimi, A. Dey, R. Jena, D. Maity and T. K. Maji, *Chem. Mater.*, 2024, **36**, 6410–6420.
18 G. E. Schukraft, R. T. Woodward, S. Kumar, M. Sachs, S. Eslava and C. Petit, *ChemSusChem*, 2021, **14**, 1720–1727.
19 S. Wang, M. Xu, T. Peng, C. Zhang, T. Li, I. Hussain, J. Wang and B. Tan, *Nat. Commun.*, 2019, **10**, 676.
20 Z. Zhan, H. Wang, Q. Huang, S. Li, X. Yi, Q. Tang, J. Wang and B. Tan, *Small*, 2022, **18**, 2105083.
21 F. Meng, J. Wang, M. Chen, Z. Wang, G. Bai and X. Lan, *ACS Catal.*, 2023, **13**, 12142–12152.
22 Y. Ma, X. Yi, S. Wang, T. Li, B. Tan, C. Chen, T. Majima, E. R. Waclawik, H. Zhu and J. Wang, *Nat. Commun.*, 2022, **13**, 1400.
23 T.-Y. Yang, Y. Zhang, G.-L. Zhang, J.-J. Zhang and Y.-H. Zhang, *Catal. Lett.*, 2023, **153**, 408–418.
24 H. Lv, R. Sa, P. Li, D. Yuan, X. Wang and R. Wang, *Sci. China: Chem.*, 2020, **63**, 1289–1294.
25 H. Zhou, C. Rayer, A. R. Antonangelo, N. Hawkins and M. Carta, *ACS Appl. Mater. Interfaces*, 2022, **14**, 20997–21006.
26 X. Chi, Z. A. Lan, Q. Chen, X. Zhang, X. Chen, G. Zhang and X. Wang, *Angew. Chem., Int. Ed.*, 2023, **62**, e202303785.
27 H. Ouyang, M. Peng, K. Song, S. Wang, H. Gao and B. Tan, *Chem. Synth.*, 2024, **4**, 50.
28 H. Ouyang, K. Song, J. Du, Z. Zhan and B. Tan, *Chem. Eng. J.*, 2022, **431**, 134326.
29 J. Li, Y. Hou, C.-X. Cui, X. Zhang, J.-C. Wang, A. Wang, Z. Chen, M. Li and T. Lou, *Dalton Trans.*, 2022, **51**, 15022–15030.
30 S.-J. Li, Y.-B. Chang, M. Li, Y.-X. Feng and W. Zhang, *RSC Adv.*, 2020, **10**, 17951–17954.
31 X. Zhang, M. Cibian, A. Call, K. Yamauchi and K. Sakai, *ACS Catal.*, 2019, **9**, 11263–11273.
32 R. Luo, M. Chen, F. Zhou, J. Zhan, Q. Deng, Y. Yu, Y. Zhang, W. Xu and Y. Fang, *J. Mater. Chem. A*, 2021, **9**, 25731–25749.
33 Q. Chen, Y. Zhang, E. You, Q. Jiang, X. Chen, Y. Wang, Z. Song, K. Chang, Z. Xie and Q. Kuang, *Small*, 2022, **18**, 2204924.
34 Y. Wu, L. Yan, Y. Yu and C. Jing, *Catal. Sci. Technol.*, 2021, **11**, 6103–6111.
35 W. Y. Gao, H. T. Ngo, Z. Niu, W. Zhang, Y. Pan, Z. Yang, V. R. Bhethanabotla, B. Joseph, B. Aguila and S. Ma, *ChemSusChem*, 2020, **13**, 6273–6277.
36 N. Das, R. Paul, S. Biswas, R. Das, R. Chatterjee, A. Bhaumik, S. C. Peter, B. M. Wong and J. Mondal, *ACS Sustainable Chem. Eng.*, 2023, **11**, 2066–2078.
37 H. Ouyang, K. Song, I. Hussain and B. Tan, *ACS Appl. Polym. Mater.*, 2023, **5**, 3574–3584.
38 W. Xu, Z. Zhang, Y. Wu, K. Chen and R. Luo, *Chem. Commun.*, 2024, **60**, 1599–1602.
39 X. Hu, L. Zheng, S. Wang, X. Wang and B. Tan, *Chem. Commun.*, 2022, **58**, 8121–8124.
40 S. Wang, K. Song, C. Zhang, Y. Shu, T. Li and B. Tan, *J. Mater. Chem. A*, 2017, **5**, 1509–1515.
41 W. Zhong, R. Sa, L. Li, Y. He, L. Li, J. Bi, Z. Zhuang, Y. Yu and Z. Zou, *J. Am. Chem. Soc.*, 2019, **141**, 7615–7621.
42 O. Buyukcakir, S. H. Je, D. S. Choi, S. N. Talapaneni, Y. Seo, Y. Jung, K. Polychronopoulou and A. Coskun, *Chem. Commun.*, 2016, **52**, 934–937.
43 X. Kang, B. Wang, K. Hu, K. Lyu, X. Han, B. F. Spencer, M. D. Frogley, F. Tuna, E. J. McInnes and R. A. Dryfe, *J. Am. Chem. Soc.*, 2020, **142**, 17384–17392.
44 R. Paul, R. Das, N. Das, S. Chakraborty, C. W. Pao, Q. Thang Trinh, G. K. Kalhara Gunasooriya, J. Mondal and S. C. Peter, *Angew. Chem., Int. Ed.*, 2023, **62**, e202311304.
45 W. Zhao, D. Zhai, C. Liu, D. Zheng, H. Wu, L. Sun, Z. Li, T. Yu, W. Zhou and X. Fang, *Appl. Catal., B*, 2022, **300**, 120719.